Cosmic Background dipole measurements with Planck-High Frequency Instrument

M. Piat[1], G. Lagache[1], J.P. Bernard[1], M. Giard[2], and J.L. Puget[1]

[1] Institut d'Astrophysique Spatiale (IAS), Université Paris Sud, Bât. 121, 91405 Orsay Cedex, FRANCE
[2] Centre d'Etude Spatiale des Rayonnements (CESR), 9 avenue du Colonel Roche BP 4346, 31028 Toulouse Cedex4, FRANCE

Received October 19, 2001; accepted ??? ??, 200?

Abstract. This paper discusses the Cosmic Background (CB) dipoles observations in the framework of the Planck mission. Dipoles observations can be used in three ways: (i) It gives a measurement of the peculiar velocity of our Galaxy which is an important observation in large scale structures formation model. (ii) Measuring the dipole can give unprecedent information on the monopole (that can be in some cases hard to obtain due to large foreground contaminations). (iii) The dipole can be an ideal absolute calibrator, easily detectable in cosmological experiments. Following the last two objectives, the main goal of the work presented here is twofold. First, we study the accuracy of the Planck-HFI calibration using the Cosmic Microwave Background (CMB) dipole measured by COBE as well as the Earth orbital motion dipole. We show that we can reach for HFI, a relative calibration between rings of about 1% and an absolute calibration better than 0.4% for the CMB channels (in the end, the absolute calibration will be limited by the uncertainties on the CMB temperature). We also show that Planck will be able to measure the CMB dipole direction at better than 1.7 arcmin and improve on the amplitude. Second, we investigate the detection of the Cosmic Far-Infrared Background (FIRB) dipole. Measuring this dipole could give a new and independent determination of the FIRB for which a direct determination is quite difficult due to Galactic dust emission contamination. We show that such a detection would require a Galactic dust emission removal at better than 1%, which will be very hard to achieve.

1. Introduction: the Cosmic Background and its dipole signal

The Cosmic Background (CB) is the extragalactic part of the diffuse electromagnetic emission at all wavelengths. If the universe obeys the cosmological principle and is homogeneous and isotropic, this background is expected to be nearly isotropic in the rest frame where the matter in a large volume around the observer has no bulk velocity other than the Hubble expansion. The measurement of the intensity and Spectral Energy Distribution (SED) of this isotropic background is a difficult observational challenge. It requires a separation of this extragalactic component from all other diffuse foregrounds (interplanetary or interstellar emission). Although the CB was detected quite early in the radio (radio-galaxies), Xrays and gamma rays as it dominates over the foregrounds, these components account for only 0.027% of the electromagnetic content of the present universe. The CB is dominated by the Cosmic Microwave Background (CMB) which accounts for 93% of electromagnetic content of the present universe and is a truly diffuse component coming from the pregalactic era of the universe. The second component in energy content is the radiation from galaxies integrated over all redshifts in the ultraviolet-optical-near-infrared (stellar emission) and in the thermal and far infrared (re-emission of stellar radiation absorbed by interstellar dust). This component has been detected only recently, first in the far infrared in the COBE-FIRAS and COBE-DIRBE data (Puget et al. 1996; Fixsen et al. 1998; Hauser et al. 1998; Lagache et al. 2000) then in the optical with HST (Bernstein et al. (in preparation, quoted by Madau & Pozzetti 2000); Pozzetti et al. 1998) and near infrared (Gorjian at al. 2000; Dwek & Arendt 1999; Cambrésy et al. 2000; Wright 2000). These measurements have been complemented by very high-energy gamma rays absorption by this CB (see for example Renault et al. 2001) but are still affected by rather large uncertainties especially in the optical and mid infrared. Figure 1 shows the spectrum of the CB from radio to gamma rays (data from Gispert et al. 2000 for the part [30nm; 1mm] and from Halpern & Scott 1999 for the radio part).

The CB should display a dipole anisotropy associated with the peculiar motion of the observer with respect to the lo-

Send offprint requests to: M. Piat, e-mail: `michel.piat@ias.u-psud.fr`

cal cosmological standard of rest. This peculiar motion has been first detected for the CMB by Kogut et al. (1993) . It is composed of several terms: the peculiar motion of the Sun (sum of the Galaxy peculiar velocity and the velocity of the Sun with the rotation of our Galaxy), the Earth velocity in its orbit around the Sun and the specific motion of the observer with respect to the Earth (orbital motion of the satellite for example). The main term is the first one with about 369 km/s in the direction $(l, b) \simeq (264.3°, 48.0°)$ (Lineweaver et al. 1996). The second one, dominated by the Earth orbital motion, is a sinusoidal term with amplitude of about 37 km/s . It is thus about 10% of the first one but has a very specific character it is perfectly known in amplitude and direction and changes periodically with time during the year. The COBE-DMR experiment has measured these terms accurately. Fixsen et al. (1996) has shown that the CMB spectrum absolutely measured with the COBE-FIRAS experiment with high accuracy could also be measured using its dipole anisotropy. The two spectra obtained were compatible within error bars. The peculiar motion of the galaxy has also been measured with respect to distant galaxies as an anisotropy in the Hubble constant (Lauer & Postman 1994). Although the accuracy is not very good, the value obtained is compatible with the one measured by COBE (Scaramella et al. 1991, Kogut et al. 1993). These measurements confirm that the rest frame defined as the one in which the CMB is isotropic coincides with the rest frame defined by the galaxies on large scales.

Motion with velocity $\boldsymbol{\beta} = \boldsymbol{v}/c$ through an isotropic radiation field of intensity $I(\nu)$ yields an observed intensity given by:

$$I_{\rm obs}(\nu, \theta) = \frac{I[\nu(1-\beta\cos\theta)]}{(1-\beta\cos\theta)^3} \qquad (1)$$

where ν is the frequency and θ is the angle between $\boldsymbol{\beta}$ and the direction of observation, these two parameters beeing measured in the observer's frame. The spectral intensity of the dipole amplitude is therefore given by:

$$\begin{aligned} I_{\rm dip}(\nu) &= I_{\rm obs}(\nu, \theta = 0°) - I_{\rm obs}(\nu, \theta = 90°) \\ &\simeq \beta\cos\theta \left(3I(\nu) - \nu\frac{{\rm d}I}{{\rm d}\nu}(\nu)\right) \text{ for } \beta \ll 1 \qquad (2) \end{aligned}$$

The spectral intensity of the CB dipole amplitude is shown in figure 1 and its relative level in figure 2.

The dipole anisotropy of the CB has a two-fold interest for future CB projects:

- At frequencies where the separation of the CB from foregrounds is difficult (from submillimeter to ultraviolet), an accurate measurement of the dipole anisotropy will give the SED of the CB independently of the interstellar and interplanetary foregrounds which do not show a dipole anisotropy.
- A very accurate measurement of the CMB dipole anisotropy over a one year period should allow to use the dipole anisotropy associated with the orbital motion of the Earth around the Sun as the best photometric calibrator for extended sources in the microwave region of the spectrum. It should therefore improve the determination of the peculiar motion of the solar system. This is possible due to the Planckian nature of the CMB and the accuracy of its temperature measured with the FIRAS spectrometer. The CMB provides today an extended photometric standard with an accuracy of less than 2 10^{-3} in thermodynamic temperature (Fixsen et al. 1996).

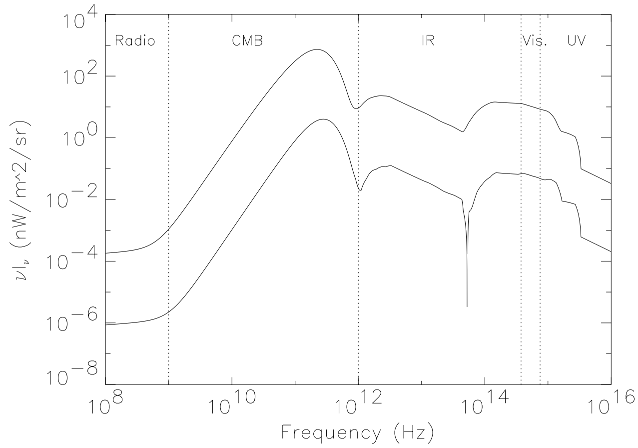

Fig. 1. Spectrum of the CB (top) and its dipole amplitude (bottom) from radio to ultra-violet.

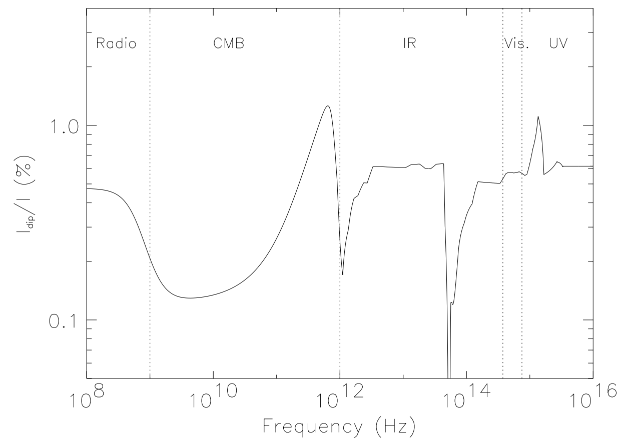

Fig. 2. Amplitude of the CB dipole relative to the CB intensity expressed in % from radio to ultra-violet.

This paper explores these two questions in the context of the Planck mission and specifically its High Frequency Instrument (Planck-HFI, Lamarre 1998). It is divided in 2 parts. The first one deals with the calibration of Planck-HFI using the CMB dipole. In section 2, we present the calibration philosophy of Planck, while section 3 concerns more specifically the calibration accuracy. The second part, in section 4, is a study of the detectability of the Far InfraRed Background (FIRB) dipole.

2. Planck-HFI calibration philosophy

Different sources will be used to monitor inflight the response or to get the photometric calibration of the Planck-HFI channels:

- Extended sources: the CMB dipole, the Earth orbital motion dipole, the Galactic disc and eventually maps of Herschel-SPIRE.
- Point sources: planets, infrared galaxies and asteroids.

A general principle throughout the calibration for all channels is that relative calibrations will be established as precisely as possible between individual scans before establishing an absolute calibration for all data.
For channels dominated by the CMB (100GHz to 217GHz), as will be seen in next section, the dipole signal from the CMB will be used to measure the relative response variations on all useful timescales since it is an extended source available all over the mission. The amplitude and direction of the cosmic dipole has been measured by COBE. It will be remeasured independantly by Planck using the dipole from the Earth orbital motion as the primary calibrator of the instrument absolute response.
For higher frequency channels, mainly dominated by galactic dust emission, the calibration will be done by comparison with COBE-FIRAS map. The absolute calibration will also be done on the whole sky. The relative variations on shorter time scales will be measured independantly and are out of the scope of this paper. A short summary of the technique is given below.
The response variation of a bolometer depends on a few fixed (or very slowly varying) parameters like the thermal conductance or the bias current for exemple. It also depends on changing parameters, mainly the temperature of the heat sink of the bolometer and the incident power background. This last quantity is directly related to the flux from the sky which is known to first order before the mission or after a first iteration on the data, and to the temperature of the various stages of the optics (1.6 K, 4K and the telescope). Since these temperatures are monitored during the mission, it will be possible to correlate the response measured as a function of time with the temperature of the relevant elements and adjust very precisely the parameter of the model describing the bolometer chain. This can be done very accurately using the slow variations of the different temperatures. This model with the temperature measurements (or any other monitored parameter found to affect the response) can be used to interpolate, if needed, the short time scale response variations on high frequency channels. Relative variations of the response will thus be established on many time scales. A preliminary absolute calibration will be built after typically a month period and will be improved until the final full data reduction for the detector is done. The bolometer model and the temperature measurements will be used to interpolate for time scales between one hour and one month.
The CMB dipole is a strong known source (using COBE data initially or its properties remeasured by Planck at the end of the mission) which can be used to monitor the response variations over various time scales for all channels where its signal either dominates or is clearly detectable. It is thus important to evaluate the achievable accuracies for both the final absolute calibration and the measurements of the relative response.

3. Using the CB dipole as a calibration signal for HFI

The CMB shows anisotropies on all scales tracing the small inhomogeneities in the pre-galactic era that lead to the formation of structure in the universe. These fluctuations are observed on a surface of last scattering as seen from the Earth. They contain high spatial frequency terms which are the main objective of the Planck mission and low frequency components which are not carrying much cosmological information as they are much more variable with the observer position (cosmic variance). The dipole term of this cosmological component is indistinguishable from the one associated with the peculiar motion of the solar system and is therefore a fundamental limit for the accuracy to measure this motion. The CMB cosmologicalanisotropies are thus defined as with no dipole component ($\ell = 1$ term of the usual decomposition in spherical harmonics of the sky). The contribution of higher ℓ to the dipole measurement is zero when it is done on the whole sky (by definition) but is not zero when the dipole is fitted on a fraction of the sky. In this section, we first present the Planck-HFI simulations we used, and explore the relative calibration on rings as well as the global absolute calibration accuracy.

3.1. Simulations

The Planck satellite will orbit around the lagrangian L2 point and will therefore follow the Earth orbital motion around the Sun. Its scanning strategy consists in rotating the satellite at 1 rpm around its spin axis which will follow the antisolar direction. The beam axis, located 85° away from the spin axis, scans the sky along large circles. We define a "circle" as beeing one instantaneous Planck observation of 1 minute. The spin axis is relocated about every hour so that each circle is scanned about 60 times covering the whole sky on six months. These 60 circles are averaged into what we call one "ring". The spin axis follows a sinusoid trajectory along the ecliptic plane with 6 oscillations per year and with full amplitude of ±10° so that the polar caps are not left unobserved.
For simplicity and to spare computer time and place, only 84 rings uniformly distributed over the sky in a one year mission were simulated. Moreover, the removal of slow drifts on circles has to be considered together with the process of removing systematic effects using redundancies and is therefore out of the scope of this paper.
The simulated sky is the sum of 5 contributions:

1. CMB cosmological anisotropies, obtained from a standard Cold Dark Matter model: $\Omega_{tot} = 1$, $\Omega_b = 0.05$, $\Omega_\Lambda = 0$ and $H_0 = 50$km/s/Mpc. The C_ℓ power spectrum is computed with CMBFAST (Seljak et al. 1996) and the map is generated in a healpix-type all-sky pixelisation with a pixel size of 3.5 arcmin (Górski et al. 1998).
2. The solar system Peculiar Motion dipole (PM dipole) assuming an amplitude of 3.36 mK in the direction $(l, b) = (264.31°, 48.05°)$ (Lineweaver et al. 1996).
3. The Earth Orbital Motion dipole (OM dipole) assuming an amplitude of about 336 μK with its maximum at zero ecliptic latitude in the direction of the OM.
4. Galactic dust, scaled from IRAS 100μm map using a 17.5K blackbody modified by a ν^2 emissivity law (Boulanger et al. 1996).
5. One realisation of the noise with levels given in table 1. These figures were estimated from the sensitivities of the Planck-HFI channels as defined by Lamarre et al. (2001). We include a $1/f^2$ contribution to the noise power spectrum with a knee frequency of 10mHz. In order to define the noise level for rings, the instantaneous sensitivity on a circle has been divided by $\sqrt{60}$, assuming that all circles are coadded into a single ring and that the noise is not correlated from one circle to the other. This is not strictly the case given the frequency aliasing produced by the co-addition (Janssen et al. 1996, Delabrouille 1998b). However, it is a rather good approximation (see figure 3 from Giard et al. 1999). Slow drifts at frequencies lower than the spin frequency $f_{\text{spin}} = 1/60$Hz are assumed to be removed by a destriping algorithm (Delabrouille 1998c).

3.2. Ring Analysis

For each rings, a linear regression is done between the simulated signal and the expected dipole signal which is the sum of the PM dipole and the OM dipole as shown on figure 3. The slope of this linear regression gives the absolute calibration factor with its uncertainty. The variations of this factor gives the relative calibration accuracy. The standard deviation of the calibration factor is therefore a good estimator of the relative calibration accuracy. The absolute calibration will be determined finally on the whole sky map (see section 3.3 for a first attempt). A mask on region with IRAS 100μm emission higher than a cut-off value can be applied in order to decrease the contribution from dust emission.

3.2.1. Relative calibration accuracy

In this analysis, we removed regions with IRAS 100μm emission higher than 10MJy/sr which is quite optimal as will be shown in 3.2.3. Figure 4 shows the variations of the calibration factor for a HFI 100GHz channel along the simulated mission assuming known OM and PM dipoles characteristics, with and without CMB cosmological anisotropies. While the PM dipole varies along the mission, the OM dipole produces almost the same signal on each rings, as shown on figure 3. The accuracy with which the dipole can be measured remains high even when the PM dipole is at its minimum, on rings around numbers 40 and 80. When CMB cosmological anisotropies are not included, the relative variations of the calibration factor are very low, mainly dominated by noise effects. CMB anisotropies dominate the uncertainties in measuring the amplitude of the dipole on individual ring. The accuracy improves with averages on larger number of rings. This part of the error goes exactly to zero when the whole sky is used. The accuracy of dipole fitting on HFI rings is therefore highly limited by the CMB cosmological anisotropies. This fit is equivalent to find the m=1 mode of the ring power spectrum Γ_m. The relation from Delabrouille et al. (1998a) links this spectrum with the C_ℓ spectrum:

$$\Gamma_m = \sum_{\ell=|m|}^{\infty} W_{\ell m} C_\ell \tag{3}$$

where $W_{\ell m}$ are window functions related to the beam shape and to the ring radius. The dipole term given by Γ_1 clearly depends on all multipole $\ell \geq 1$ of the CMB cosmological anisotropies. This coupling between modes disappear on a full map, indicating that the final absolute calibration should be done on the full map of Planck data as illustrated in section 3.3. Nevertheless, relative calibration between rings at 100GHz is expected to be possible at a level of the order of a few percent as discussed in 3.2.3. On 545GHz calibration data shown on figure 5, the signal is dominated by galactic dust emission and the accuracy of the CMB dipole calibration is about the same considering or not CMB cosmological anisotropies. The relative calibration between rings at 545GHz is possible at a level of about 15%.

3.2.2. Shifted direction of the CMB dipole

The PM velocity vector direction is known with an accuracy of about 14 arcmin at 1σ (Lineweaver et al. 1996). To test the effect of this uncertainty on rings relative calibration, we fit the simulated data with a shifted PM dipole by 30 arcmin in all directions (about 2σ from COBE results). Figure 6 shows the results obtain close to the worst case. The accuracy on the relative calibration is not highly affected and the calibration factor standard deviation is increased by only 15%. These results show that a relative calibration on rings is still possible in an iterative way: with a first step relative response correction and with enough observation time, the dipole direction will be improved and therefore the relative calibration will be enhanced.

3.2.3. Effect of dust contamination

The effect of dust contamination on calibration can be tested by removing from the dipole fit the data points

Table 1. Expected sensitivities of Planck-HFI per detection chain. The last two lines give the expected sensitivities per channel for the full mission.

Frequency (GHz)	857	545	353	217	143	100
Resolution (arcmin)	5	5	5	5	7.1	9.2
Number of detector	4	4	4	4	4	4
$NET_{\rm CMB}$ (μK.Hz$^{-0.5}$)	182000	3995	553	182	123	99
Thermo. temperature sensitivity per ring (μK)	199000	4370	605	200	113	80
NEI (MJy.sr^{-1}.Hz$^{-0.5}$)	$269\,10^{-3}$	$232\,10^{-3}$	$165\,10^{-3}$	$88\,10^{-3}$	$47\,10^{-3}$	$23\,10^{-3}$
Intensity sensitivity per ring (MJy.sr^{-1})	$294\,10^{-3}$	$253\,10^{-3}$	$180\,10^{-3}$	$96\,10^{-3}$	$43\,10^{-3}$	$19\,10^{-3}$
Thermo. temperature sensitivity full mission (μK)	36500	801	111	37	17	11
Intensity sensitivity full mission (MJy.sr^{-1})	$54\,10^{-3}$	$46\,10^{-3}$	$33\,10^{-3}$	$18\,10^{-3}$	$6.6\,10^{-3}$	$2.6\,10^{-3}$

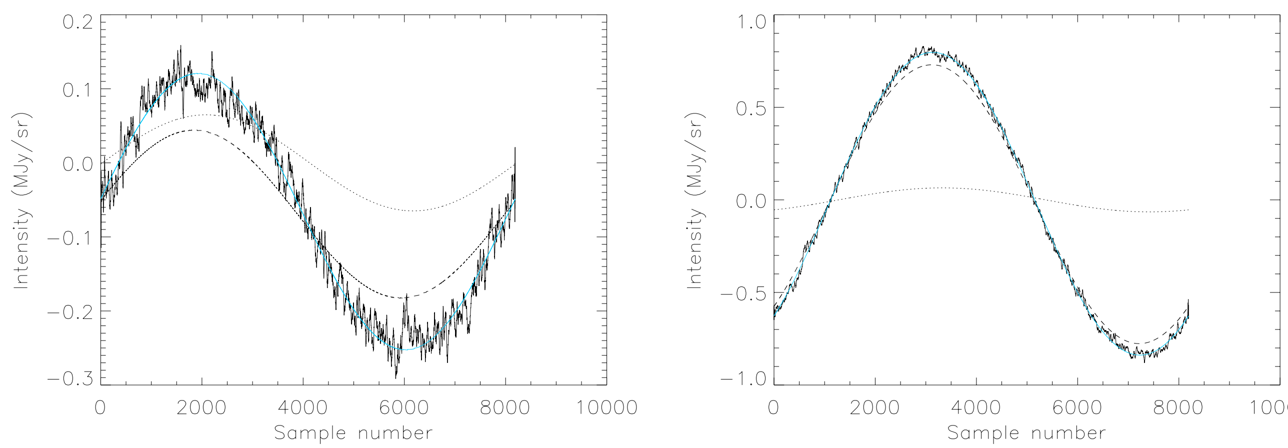

Fig. 3. Example of the analysis realised on two rings. The black solid curve is the simulated signal. The OM and PM dipoles are represented by dotted and dashed curves respectively. The grey curve is the OM plus PM motion dipole fitted on the signal.

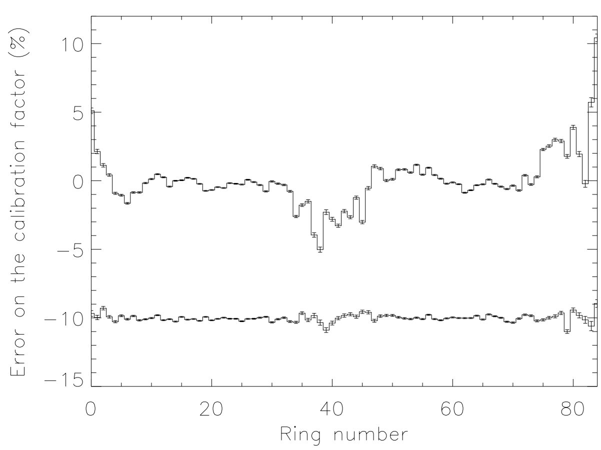

Fig. 4. Variations of the calibration factor for a HFI 100GHz channel as a function of the simulated ring number. We have assumed perfectly known OM and PM dipoles characteristics. The lower curve has been computed without CMB cosmological anisotropies and is shifted by 10% for clarity. Regions where IRAS 100μm emission greater than 10MJy/sr were removed from the fit.

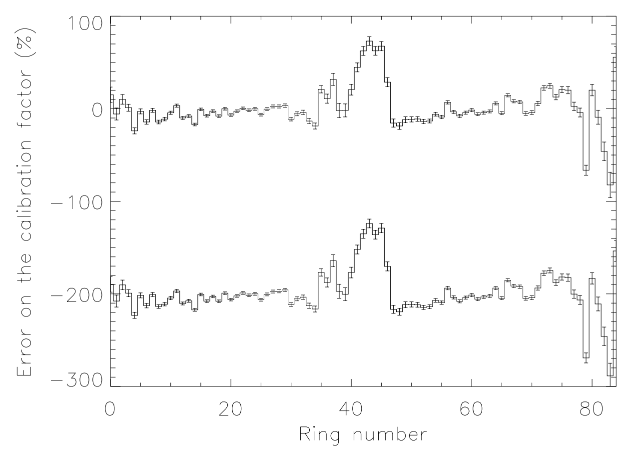

Fig. 5. Variations of the calibration factor for a HFI 545GHz channel as a function of the ring number. The legend is similar to figure 4. The lower curve is shifetd by 200% for clarity.

having an excess emission in IRAS 100μm map. For very low cut-off values, the fit is degraded due to the decrease in the number of data points. On the other hand, with a high cut-off value, all the emission of dust in our Galaxy is taken into account in the fit and it degrades the final accuracy. We therefore expect an optimum value to exist in between. In order to study this effect, the standard de-

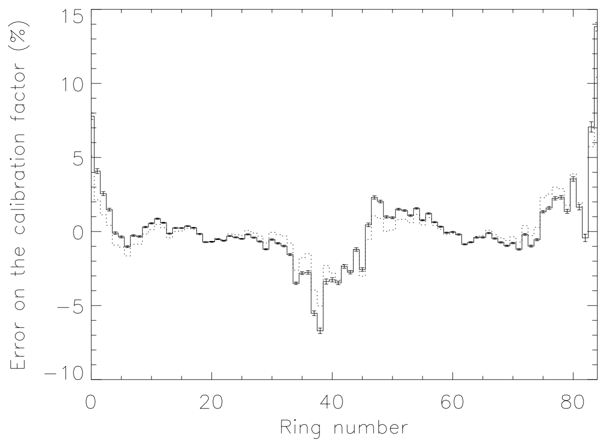

Fig. 6. Variations of the calibration factor for a HFI 100GHz channel as a function of the ring number with an error in the PM dipole direction of 30 arcmin. The dotted curve assumed a perfect known PM dipole direction. Regions where IRAS $100\mu m$ emission greater than 10MJy/sr were removed from the fit.

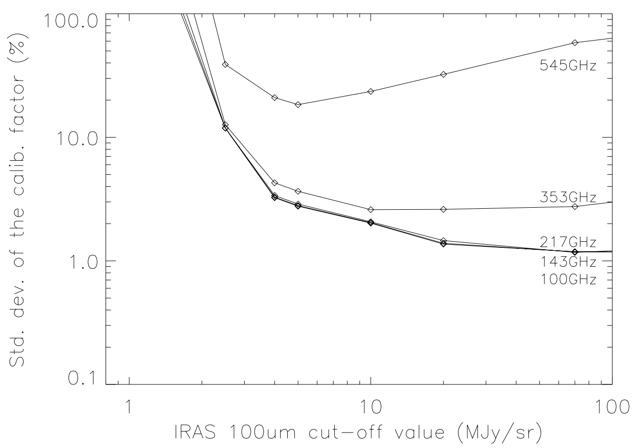

Fig. 7. Variations of the standard deviation of the calibration factor (expressed in percentage of the calibration factor) for all HFI channels, except the 857GHz, as a function of the IRAS $100\mu m$ cut-off value.

viation of the calibration factor on all rings is plotted in figure 7 as a function of the IRAS $100\mu m$ cut-off.

On CMB channels (100GHz, 143GHz and 217GHz), increasing the IRAS $100\mu m$ cut-off value do not decrease the relative calibration accuracy: as shown in previous section, this accuracy is limited only by CMB cosmological anisotropies. A relative calibration accuracy of 1.2% at 1σ is possible on these channels. On higher frequency channels, the emission of galactic dust is more dominant and there is, as expected, an optimum cut-off value at a few MJy/sr.

3.3. Absolute calibration accuracy on all simulated data

In order to test the accuracy of absolute calibration on a global map, we have fitted simultaneously all simulated rings with a dipole term from OM and PM. This is an approximation of a full fit on the whole sky. Our procedure nevertheless gives a first approach to the global calibration which will be expensive in computer resources.
We can write the signal as:

$$\mathrm{Signal}(l,b) \;=\; F \times [\mathrm{PM}_{(A_0,l_0,b_0)}(l,b) + \mathrm{OM(l,b)} \quad (4)$$
$$+\mathrm{Gal}(l,b) + \mathrm{CMBA}(l,b)] \quad (5)$$

where F is the calibration factor, A_0 is the PM dipole amplitude (A_0=3.36 mK), (l_0, b_0) is the PM dipole direction ($l_0 = 264.31°, b_0 = 48.05°$), Gal is the Galactic signal and CMBA the CMB anisotropy contribution. This analysis has been done only on CMB channels (100GHz, 143GHz and 217GHz). In order to remove dust contamination effect, we choose an IRAS $100\mu m$ cut-off value of 15MJy/sr. Morevover, we remove CMB cosmological anisotropies from the fit since, in our case, they introduce a ℓ =1 term which will not be present when using the whole sky. We assume in the procedure that we perfectly know only the OM dipole so that the calibration is due to this term. We first search for the best F, A_0, l_0 and b_0 and their accuracy by fitting simultaneously the 84 rings signal of one CMB channel. This analysis shows that we can separate our problem into two much faster fitting procedures: one to get the best calibration factor and PM dipole amplitude, and the other to find the best PM dipole direction and amplitude. This two problems are mostly decorelated since a change in the PM dipole direction cannot be compensated by a change in its amplitude (or in the calibration factor). These two analysis lead to χ^2 contour plot shown in figure 8 and 9. We obtain the following results for one 100GHz detection chain:

- We can recover the PM dipole direction at better than 1.7 arcmin (Fig. 8).
- We find $A_0 = (3.374 \pm 0.007)$ mK at 95% CL and
- F is found to be equal to 0.996 ± 0.002 at 95% CL (Fig. 9).

This shows on the one hand that Planck-HFI will be able to make a new and accurate determination of the PM dipole direction. On the other hand, by combining the error on F and A_0 and considering the OM dipole as an absolute calibrator, we see that we can make an HFI low frequency absolute calibration at better than 0.4%. This first attempt is moreover quite pessimistic since it takes into account only part of Planck-HFI one year data.

4. Detectability of the dipole effect in the Far InfraRed Background (FIRB)

The FIRB is due to the integrated emission of distant redshifted galaxies. Its SED between 100μm and 1mm is

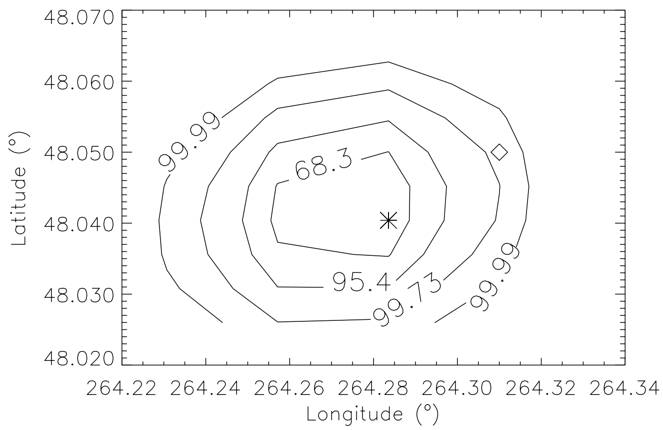

Fig. 8. Contour plot in the l/b plan of the χ^2 obtained with the fit of the PM dipole direction, expressed in percentage of confidence level, for a 100GHz channel. We assumed known PM dipole amplitude and instrument response for this fit, and no CMB cosmological anisotropies (see text). The asterisk point represents the best fit while the diamond is the input dipole direction. Regions with IRAS 100μm emission higher than 15 MJy/sr were removed from the fit.

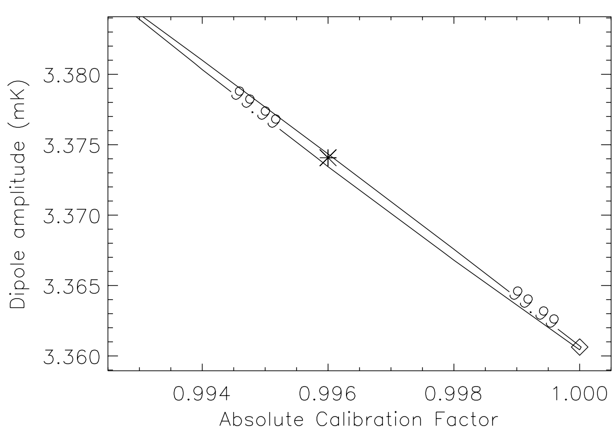

Fig. 9. Contour plot in the F/A_0 plan of the χ^2 obtained with the fit of the PM dipole amplitude and instrument response, expressed in percentage of confidence level, for a 100GHz channel. We assumed a known dipole direction for this fit, and no CMB cosmological anisotropies (see text). The asterisk point represents the best fit while the diamond is the input simulation. Regions with IRAS 100μm emission higher than 15 MJy/sr were removed from the fit.

well represented by the following expression (Lagache et al. 1999):

$$I(\nu) = 8.8\,10^{-5} \left(\frac{\nu}{\nu_0}\right)^{1.4} P_\nu(T_0) \quad (6)$$

where $\nu_0 = 100cm^{-1}, T_0 = 13.6K$ and $P_\nu(T)$ is the Planck function. This expression has been obtained by averaging over multiple clean region, almost homegenously distributed on the sky, where dust contamination is expected to be negligible. We therefore assumed that it represents the SED of the FIRB at rest. The FIRB dipole spectrum can be deduced from its monopole spectrum by using equation 2 and 6:

$$I_{\mathrm{dip\,FIRB}}(\nu) = \beta I(\nu) \left(\frac{x \exp x}{\exp x - 1} - 1.4\right) \quad (7)$$

where $x = h\nu/(kT_0)$.

4.1. Signal to Noise ratio

In order to evaluate the expected sensitivity of HFI on the FIRB dipole signal, we first consider the case of instrumental noise having a pure white spectrum. As for the CMB dipole, the FIRB dipole will be best detected on a full sky map where no aliasing from CMB anisotropies will occur. An estimation of the Signal-to-Noise Ratio (SNR) can be done on the $\ell = 1$ multipole of the angular power spectrum decomposition. The expected C_1 for a dipole signal having an amplitude A is given by:

$$C_1 = \frac{4\pi}{9} A^2 \quad (8)$$

Knox (1997) and Tegmark (1997) have shown that the effect of uniform instrumental noise can be accurately modeled as an additional random field on the sky, with an angular power spectrum given by:

$$C_{\ell\,\mathrm{noise}} = \Omega_b \sigma^2 \quad (9)$$

where Ω_b is the beam solid angle and σ is the r.m.s. noise per pixel. The SNR on C_1 is therefore equal to $SNR = C_1/C_{1\,noise}$ and the results are summarised in table 2. It shows that the FIRB dipole can be detected at 857GHz and 545GHz but not at 353GHz. Even an averaging over 10° could allow to detect the FIRB dipole effects with a significative SNR on these two high frequency channels if the detection noise is white.
Nevertheless, the HFI will exhibit 1/f noise mainly due to the readout electronics (Gaertner et al. 1997, Piat et al. 1997), temperature fluctuations of the cryogenic system (Piat et al. 1999) and from far side lobe signal (Delabrouille 1998b). The required knee frequency is 10mHz for HFI in order to have enough stability on a timescale of 1 minute corresponding to the spin period of the satellite (Piat et al. 1999). Destriping algorithm can remove an important fraction of low frequency drifts. Delabrouille (1998c) has shown that removing fluctuations on timescales larger than the spinning period of Planck is possible thanks to redundancies. A conservative analysis could be made by assuming that all slow components of the noise, except frequencies lower than the spin frequency, are not filtered. Equation 3 allows to express the ring anisotropy power spectrum Γ_m with the C_ℓ angular power spectrum on the sky. The window functions $W_{\ell m}$ are given by (Delabrouille et al. 1998a):

$$W_{\ell m} = B_\ell \mathcal{P}^2_{\ell m}(\Theta) \quad (10)$$

Table 2. FIRB dipole level in the Planck-HFI channels and SNR for three pixelisations assuming a white detector noise only. We also assumed a 1.17 year mission, square pixels with size given by FWHM and bolometer noise given on table 1.

Frequency (GHz)	857	545	353
FIRB dipole intensity amplitude (MJy/sr)	$1.6\,10^{-3}$	$3.4\,10^{-4}$	$4.9\,10^{-5}$
SNR per pixel	0.04	0.01	0.00
SNR per pixel of 1°	0.50	0.12	0.2
SNR per pixel of 10°	5.0	1.2	0.2
$C_{1\,\mathrm{FIRB}}$ $((MJy/sr)^2.rad^2)$	$3.5\,10^{-6}$	$1.7\,10^{-7}$	$3.4\,10^{-9}$
$C_{1\,\mathrm{noise}}$ $((MJy/sr)^2.rad^2)$	$6.1\,10^{-9}$	$4.6\,10^{-9}$	$2.3\,10^{-9}$
SNR full map on C_1	565	36	1.5

where Θ is the ring angular radius, B_ℓ is the beam response function (assuming a symmetric beam) and $\mathcal{P}_{\ell m}$ are given by the following expression where $P_{\ell m}$ are the associated Legendre polynomials:

$$\mathcal{P}_{\ell m}(\theta) = \sqrt{\left(\frac{2\ell+1}{4\pi}\right)\frac{(\ell-m)!}{(\ell+m)!}}\,P_{\ell m}(\cos\theta), \quad \text{for } m \geq 0,$$
$$= (-1)^{|m|}\mathcal{P}_{\ell|m|}(\theta), \quad \text{for } m < 0,$$

Equation 3 can be used to deduce the angular power spectrum of the instrumental noise from the Noise Equivalent Power (NEP) spectrum.
A mode m on a ring has an equivalent frequency bandwidth of $1/(2T_{spin})$ where T_{spin} is the spin period. Furthermore, the NEP has to be filtered by the beam in order to obtain the noise spectrum projected on the sky. The NEP is therefore related to the ring power spectrum of the noise by:

$$NEP^2(f)B^2(f) = 2T_{\mathrm{spin}}\Gamma_m \tag{11}$$

where $f = m/T_{\mathrm{spin}}$ is the frequency. $B(f)$ is the beam filter given by the following expression in the case of a gaussian beam shape of Full Width Half Maximum $FWHM = \sigma_b\sqrt{8\ln 2}$:

$$B(f) = \exp\left[-\frac{1}{2}\left(f\frac{\sigma_b T_{\mathrm{spin}}}{\sin\Theta}\right)^2\right] \tag{12}$$

Equation 3 can therefore be expressed in terms of NEP:

$$NEP^2(f = m/T_{\mathrm{spin}}) = \frac{2T_{\mathrm{spin}}}{B^2(f)}\sum_{\ell=|m|}^{\ell_{\max}} C_{\ell\,\mathrm{noise}}W_{\ell m} \tag{13}$$

where the sum is done on all accessible ℓ. The value of $\ell_{\max}$ is given by the highest frequency $f_{\max}$ transmitted by the readout electronics, about 100Hz for HFI that leads to $\ell_{\max} = T_{\mathrm{spin}}f_{\max}/\sin\Theta = 6000$ for a ring angular radius $\Theta = 90°$.
Equation 13 can be viewed as a matrix multiplication:

$$NEP^2 = M \times C_{\mathrm{noise}} \tag{14}$$

where NEP and C_{noise} are vectors containing $NEP(f = m/T_{\mathrm{spin}})$ and $C_{\ell\,\mathrm{noise}}$ respectively. M is a triangular matrix since Γ_m depends only on C_ℓ with $\ell \geq |m|$, and the solution is therefore quite easy to obtain. With this method, we get $C_{\ell\,\mathrm{noise}}$ assuming a noise spectrum of Planck-HFI given by:

$$NEP^2(f) = NEP_0^2\left[1 + \left(\frac{f_{\mathrm{knee}}}{f}\right)^\alpha\right] \tag{15}$$

where NEP_0 is the NEP value in the white part of the noise, f_{knee} is the knee frequency and α a constant. The effect of $1/f$ noise on the angular power spectrum is shown on figure 10 for a knee frequency of 10mHz in 4 different cases of noise behaviour. The SNR on C_1 will be degraded by a maximum factor of about 270 which nevertheless allows a detection at more than 2σ at 857GHz if foregrounds would be negligible..

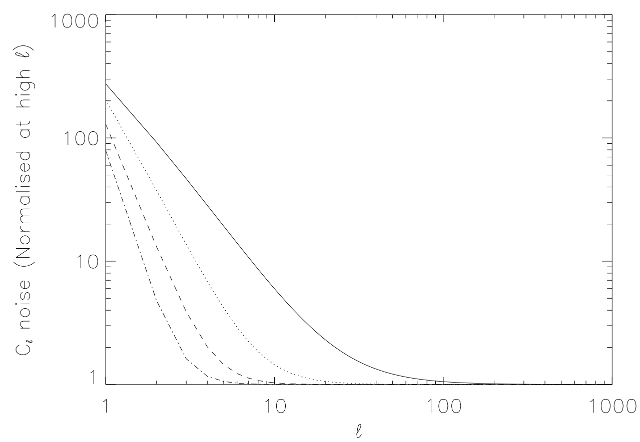

Fig. 10. Effect of $1/f$ noise on the noise angular power spectrum $C_{\ell\,\mathrm{noise}}$ normalised at high ℓ, for a knee frequency of 10mHz. The solid curve correspond to a power $\alpha = 1$ (see equation 15) while the dotted, dashed and dot-dashed lines are for $\alpha = 2$, 3 and 4 respectively.

4.2. Estimation of the total dipole spectrum

In order to evaluate the effect of calibration and component separation, the relative level of FIRB dipole with respect to other components has to be evaluated. The total dipole signal on Planck-HFI channels is produced by the CMB, the FIRB and also from the inhomeneously dust distribution in the Galaxy.
The repartition of dust in the Galaxy produces a dipole

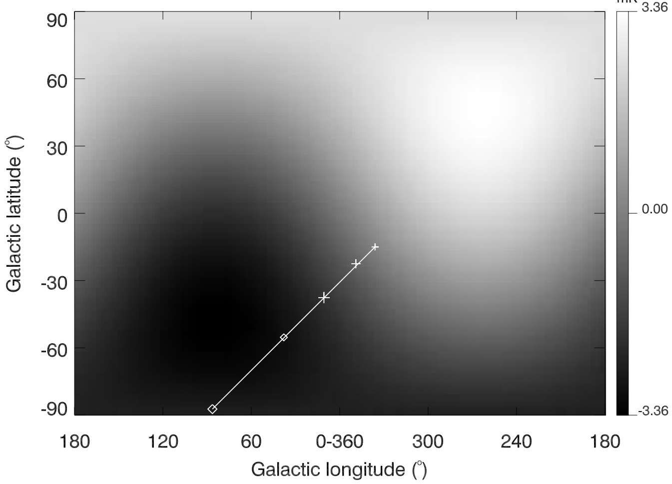

Fig. 11. Dust dipole directions superposed to the CMB dipole. The crosses are points obtain with COBE-DIRBE data at 100μm, 140μm and 240μm with increasing size of the symbol, assuming a cut in galactic latitude of $\pm 15°$. These points have been extrapolated to HFI 350μm (857GHz) and 550μm (545GHz) channels represented by diamonds with increasing size.

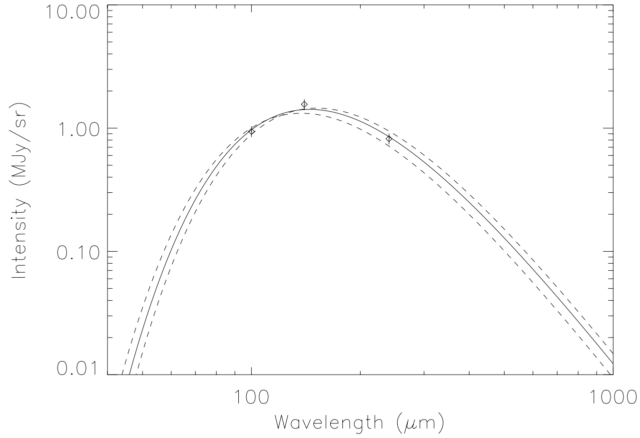

Fig. 12. Spectrum of the dust dipole. The diamonds are the points obtain with COBE-DIRBE assuming a cut in galactic latitude of $\pm 15°$. The solid line is the best fit with a λ^{-2} emissivity leading to a dust temperature of (20$\pm$1)K and a H I column density of $(5.2 \pm 1.5)\,10^{19}\text{cm}^{-2}$. Dashed lines gives the upper and lower limits.

signal, the so-called "dust dipole", that is not due to Doppler effect. This signal has been estimated on COBE-DIRBE sky map at 100μm, 140μm and 240μm. In order to remove strong emission from the galactic plane, a cut in galactic latitude or a cut-off in maximum emission level has been applied. Both methods leads to about the same results for intermediate cut, within less than 20° on the fitted dipole direction and about 10% accuracy on its amplitude. The dipole that dust mimic is push toward the galactic south pole as the cut in the latitude is increased, or the cut-off in maximum emission is decreased. A reasonnable cut in galactic latitude of $\pm 15°$ has therefore been applied. These data have been used in order to interpolate the dust dipole on Planck-HFI 545GHz and 857GHz as shown on figures 11 and 12. The dipole direction has been extrapolated linearly with galactic coordinate, assuming a $\pm 20°$ uncertainty. It seems to go in the direction of the south galactic pole, meaning that at higher wavelength only the north/south disymmetry will be seen. The dust dipole spectrum follows a (20 ± 1)K blackbody modified by a ν^2 emissivity and with a H column density of $(5.2 \pm 1.5)\,10^{19}\text{cm}^{-2}$. We also assumed that 10% of this signal can be removed by component separation. The resulted dust dipole spectrum with its uncertainty, projected on the CMB dipole axis, is shown on figure 13 together with the CMB, FIRB and total dipole. The FIRB dipole signal is only about 10% of the total dipole dominated by the dust emission one for frequencies higher than 700GHz, which has two consequences:

1. To recover the FIRB dipole signal, the dust dipole has to be removed by componenent separation to a 1% level accuracy (10 times better) which will be difficult to achieve, even on large scales.

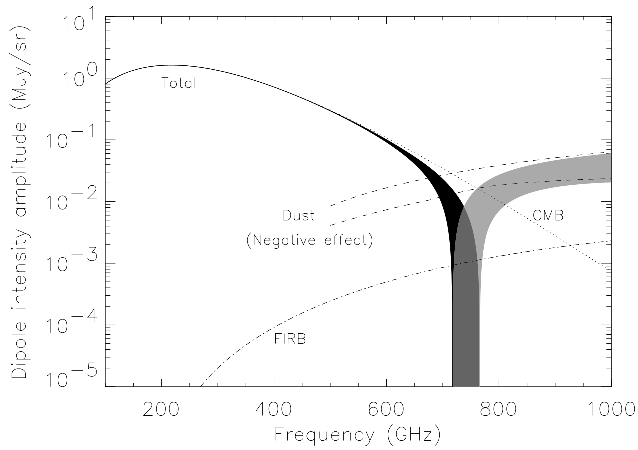

Fig. 13. SED of dipoles from the CMB (dotted line), dust (dipole projected on the CMB dipole direction, dashed lines giving lower and upper limits) and the FIRB (dot-dashed line). The solid region gives the spectrum of the total dipole with the uncertainty on the dust dipole, the black one beeing for positive dipole while the grey one is for negative dipole.

2. The calibration on the 545GHz and 857GHz channels will be obtained by comparison of the galactic plane emission measured with COBE-FIRAS. The accuracy on these channels will probably be limited by the COBE-FIRAS calibration accuracy which is about 3%, a factor 3 higher than needed to detect the FIRB dipole effect.

The detection by Planck-HFI of the FIRB dipole is therefore unfortunately very difficult, due to component separation and calibration accuracies of the high frequency channels.

5. Conclusion

We have shown that we can use the PM and OM dipoles observation for relative and absolute calibration for Planck-HFI. On CMB channels, we reach a relative calibration accuracy of about 1.2% on rings and an absolute calibration accuracy better than 0.4% when the whole sky is used. Moreover, the CMB dipole direction will be improved by Planck. At the end, the Planck-HFI absolute calibration will be limited by the uncertainty on the CMB temperature. The next step consist of a detail study of systematics effects on calibration.

The detectability of the FIRB dipole has also been studied and we have shown that it will be a difficult challenge due to dust contamination.

References

Boulanger F., Abergel A., Bernard J.P. et al., 1996, A&A 312, 256.

Cambrésy L., Reach W.T., Beichman C.A., Jarrett T.H., 2000 ApJ 555, 563

Delabrouille J., Górski K.M., Hivon E., 1998, MNRAS, 298, 445.

Delabrouille J., 1998, Ph. D. thesis.

Delabrouille J., 1998, A&A Sup. Ser. 127, 555

Dwek E., Arendt R.G., Hauser M.G., Fixsen D. et al., 1998, ApJ, 508, 106

Fixsen D.J., Cheng E.S., Gales J.M. et al. 1996, ApJ 473, 576

Fixsen, D.J., Dwek, E., Mather, J.C. et al. 1998, ApJ 508, 123

Gaertner S., Benoit A., Lamarre J.M. et al., 1997, A&A Sup. Ser. 126, 151

Giard M., Hivon E., Nguyen C. et al., 1999, astro-ph/9907208

Gispert, R, Lagache, G., Puget, J. L, A&A 360, 1

Gorjian V., Wright E.L., Chary R.R., 2000, ApJ, 536, 550

Górski K.M., Hivon E., Wandelt B.D., 1998, in proceedings of the MPA/ESO cosmology conference, "Evolution of Large Scale Structure", A.J. Banday, R.S. Sheth, L. Da Costa eds.

Halpern M. & Scott D., astro-ph/9904188

Hauser, M.G., Arendt, R.G., Kelsall, T. et al., 1998, ApJ 508, 25

Janssen M., Scott D., White M. et al., 1996, astro-ph/9602009

Knox L., 1995, Phy. Rev. D, vol. 52, Issue 8, 4307

Kogut A., Lineweaver C., Smoot G.F. et al., 1993, ApJ 419, 1

Lagache G., Abergel A., Boulanger F. et al., 1999, A&A 344, 322.

Lagache, G., Haffner, L. M., Reynolds, R. J., Tufte, S. L., 2000, A&A 354, 247

Lamarre J.M., 1998, Proc. of the workshop on The Cosmic Microwave Background and the Planck mission, 22-26 June 1998, Santander, Spain.

Lamarre J.M., 2001, HFI Instrument Working Group, 27-28th September 2001 held in IAS, Orsay, France.

Lauer T.R., Postman M., 1994, ApJ 425, 418.

Lineweaver C.H., Tenorio L., Smoot G.F. et al., 1996, ApJ 470, 38.

Madau P., Pozzetti L., 2000, MNRAS 312, 9

Piat M., Lamarre J.M., Benoit A. et al., 1997, Proc. 7th Int. Workshop on Low Temperature Detectors LTD-7, 27 July - 2 August 1997, Munich, Germany, pub. by MPI Physik, ISBN 3-00-002266-X, avail. from urg@mppmu.mpg.de

Piat M., Leriche B. Torre J.P. et al., 1999, NIMA 444, 413-418

Pozzetti L., Madau P., Zamorani G., et al., 1998, MNRAS 298, 1133

Puget, J.L., Abergel, A., Bernard, J.P. et al. 1996, A&A 308, L5

Renault, C., Barrau, A., Lagache, G., Puget, J.-L., A&A, 371, 771

Scaramella R., Vettolani G., Zamorani G., 1991, ApJ 376, L1

Seljak U., and Zaldarriaga M., 1996, ApJ 469, 437

Tegmark M., 1997, Phy. Rev. D, vol. 56, Issue 8, 4514

Wright E.L., 2001, ApJ in press

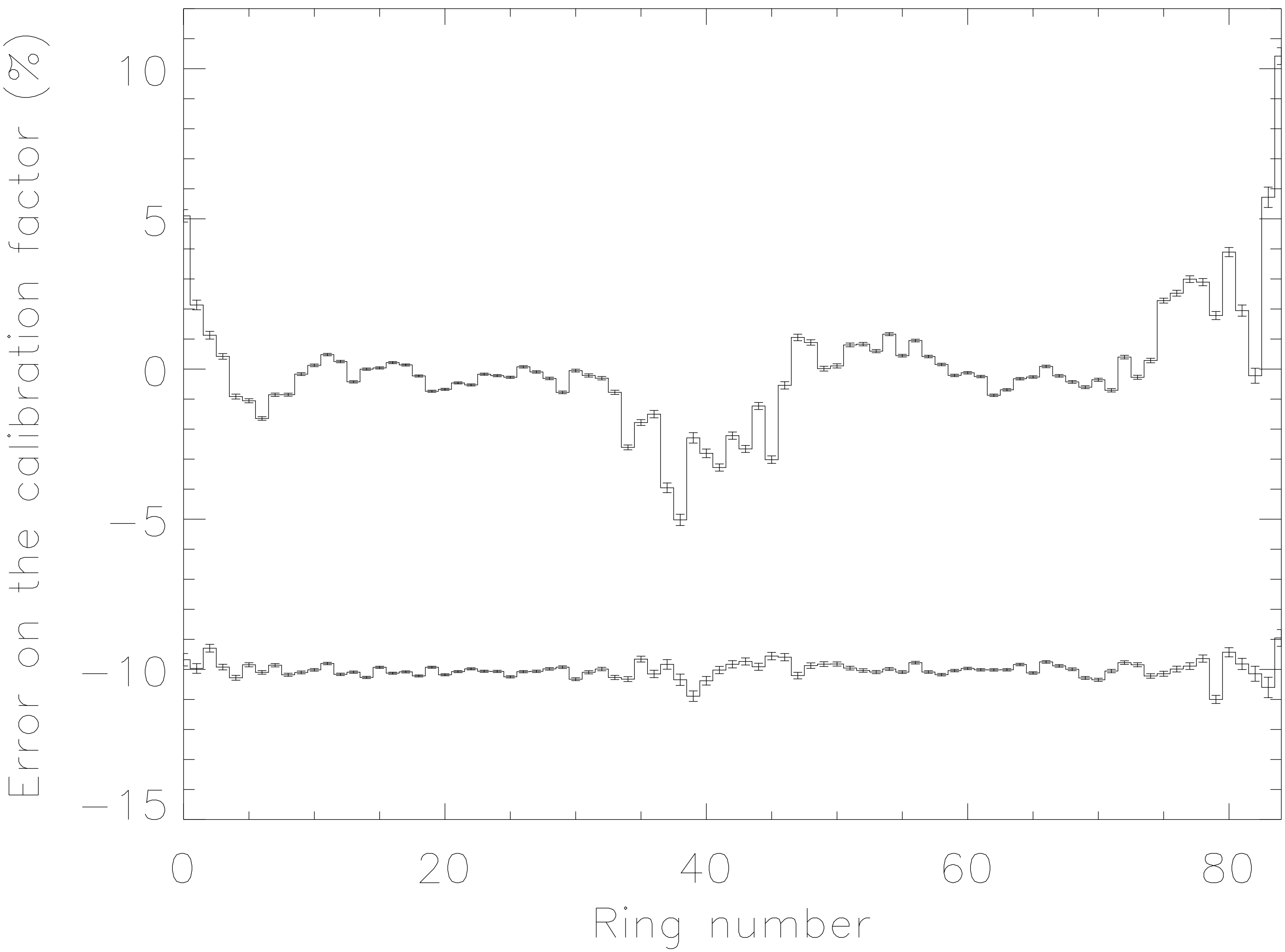
Error on the calibration factor (%)
10
5
0
−5
−10
−15
0
20
40
60
80
Ring number

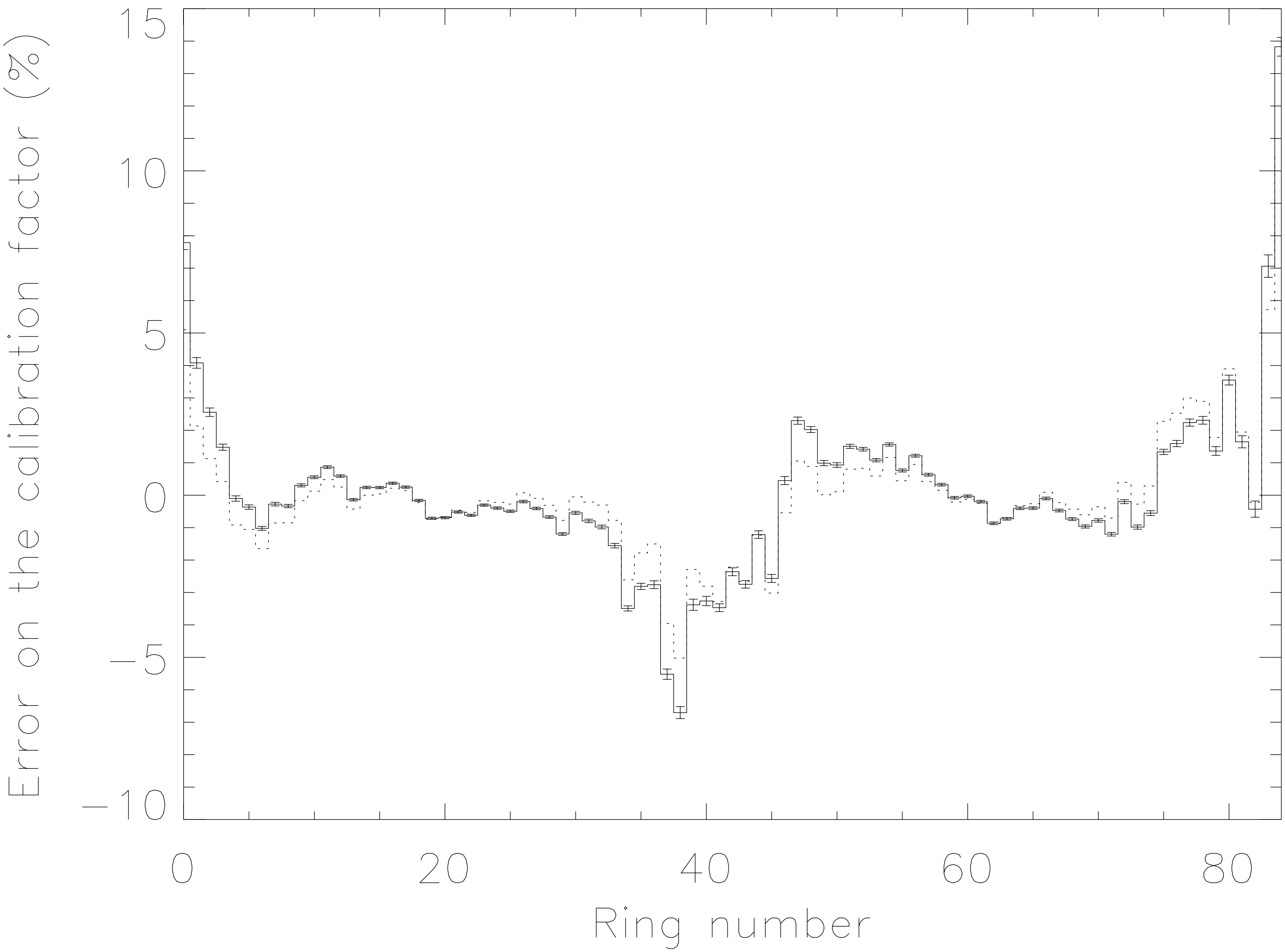
Error on the calibration factor (%)
15
10
5
0
−5
−10
0
20
40
60
80
Ring number

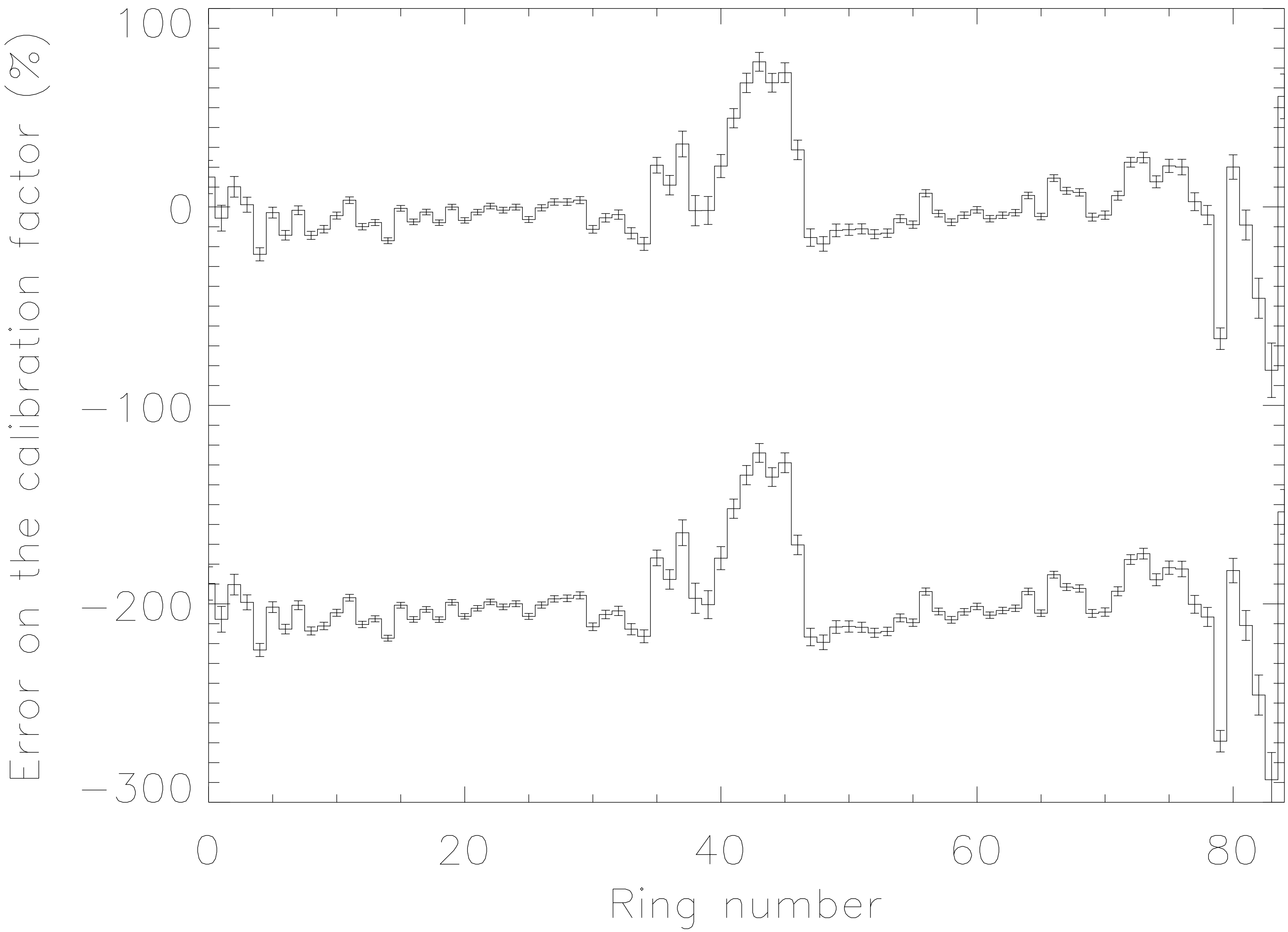
Error on the calibration factor (%)
100
0
−100
−200
−300
0
20
40
60
80
Ring number

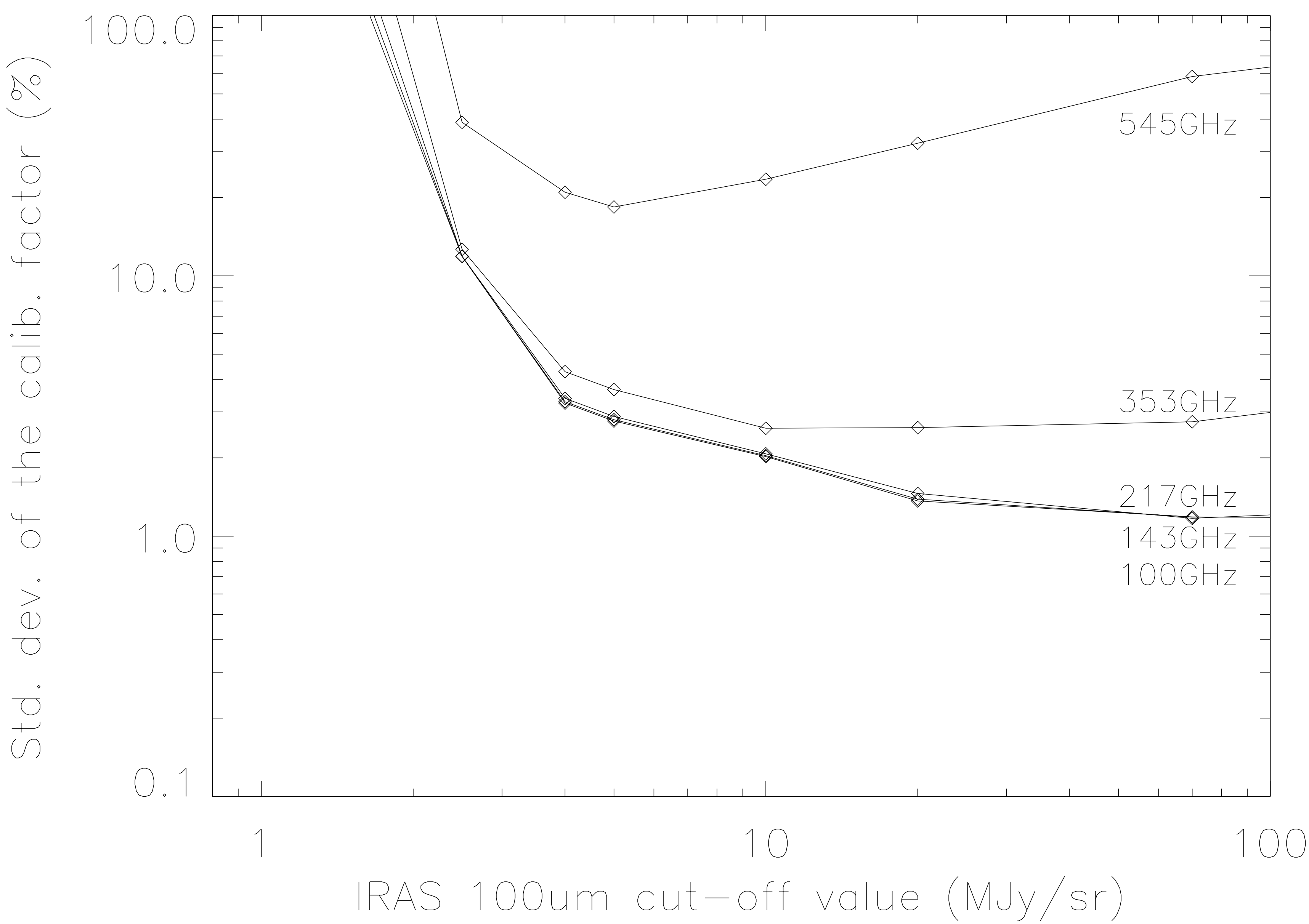
Std. dev. of the calib. factor (%)
100.0
10.0
1.0
0.1
1
10
100
IRAS 100um cut-off value (MJy/sr)
545GHz
353GHz
217GHz
143GHz
100GHz